Eidgenössische Technische Hochschule Zürich
Swiss Federal Institute of Technology Zurich

Towards a ballistic gravimeter based on Paul trap

Quantech Workshop Report

Yu Liu, Yuchen Zhao, Giovanni Vio
yuliuy@student.ethz.ch
yuczhao@student.ethz.ch
giovio@student.ethz.ch

Photonics Lab
ETH Zürich

Supervisors:
Dr. Martin Frimmer (Photonics Lab)
Prof. Lukas Novotny (Photonics Lab)

September 17, 2026

Abstract

Measurement of gravitational acceleration is crucial in fields such as geology and archaeology. Although current measurement techniques using free-falling mirrors or atom clouds easily achieve sensitivity to 10^{-8} m/s^2, the bulky mechanical and optical designs limit the utility of such devices. To develop a device that is theoretically comparable in sensitivity, more compact, and lower in cost, we proposed, built, and tested a prototype of a new type of gravimeter using charged nanoparticles and a Paul trap. With a newly designed Paul trap featuring vertical optical access, we recorded approximately a 14 mm in total fall of a single nanoparticle with the acceleration as 0.24 m/s^2 during the first half of falling. Analysis of the falling trajectory shows that it is modulated by the axial electric field induced by the Paul trap, which is caused by the slow switching off speed of electronics and local minimums of trapping potential. In the second half of the fall, the nanoparticle oscillates strongly before resting at the bottom, with a damping coefficient comparable to that of a harmonic oscillator in the same vacuum environment, indicating that gravity dominates over all other forces when the electronics are fully switched off. However, the camera resolution and refreshing rate limit the extraction of acceleration in this region. Future development of detection system and electronics should enable a much preciser measurement of gravitational acceleration. This work explores the possibility of a novel gravimeter and lays the engineering foundation for the Paul trap based gravimeter.

Contents

Chapter 1

Introduction

In order to provide the reader with a motivation for our project, we will begin this chapter with a general introduction on gravimeters and in particular to ballistic gravimeters, highlighting the limitations of the devices currently available on the market. These limitations will act as a motivation for our project, which will be presented, in its idea and goals, in section 1.3 of this chapter. In section 1.4, a first experiment testing the feasibility of our idea will be illustrated, acting as a motivation for the later development and engineering of the device, which will be presented in the second chapter.

1.1 Ballistic gravimeters

A gravimeter is a sensor used to measure the gravitational acceleration at the Earth's surface. It finds a wide range of applications, from geology to archaeology, exploiting the fact that the value of the gravitational acceleration is not constant across the Earth's surface, and depends on, among others, topographical features, underground mineral composition and presence of magma [1][2]. Table 1.1 illustrates as an example the sensitivities required by such sensor in order to be used for different applications.

Detectable feature	Required sensitivity [µGal]
Hönggerberg hill	10^5
Archaeological findings	10^1
Soil moisture	10^0

Table 1.1: Example of required sensitivity of a gravimeter in order to detect given features [3]. A µGal, common measurement unit in the field of gravimetry, corresponds to 10^{-8} m/s^2.

Various types of gravimeters exist, based on different working principles. To name the most important ones: atom interferometry gravimeters [4], MEMS-based gravimeters [5] and ballistic gravimeters [6].

We will now illustrate the working principle of ballistic gravimeters. They exploit what is probably the most straightforward way to measure gravity: dropping a macroscopic object in vacuum and measuring its position with time. The value of the gravitational acceleration can then be extracted by fitting the well known kinematic formula for the position of a free mass under a constant acceleration applied:

$$x = \frac{1}{2}at^2 + v_0 t$$

where a is the value of the acceleration, t time and v_0 the initial velocity of the body. We are implicitly setting the initial position of the body at zero.

1.2 State-of-the-art: the FG5-X

Although their working principle might sound simple, ballistic gravimeters are used and comparable in performance to other available gravimeters in the market. Among them, the current state of the art is represented by the "FG5-X" by the Colorado-based company "Micro g LaCoste" [7]. We will therefore now present this specific device with the goal of understanding its features and limitations.

Figure 1.1 illustrates a schematics of the FG5-X gravimeter. The device works by letting a mirror free-fall into a vacuum chamber. During the fall, an interferometric laser system is used to precisely track the position of the mirror with time, exploiting the reflection of the laser on the falling mirror itself. After a fall of 33 cm, a mechanical system catches the mirror in-flight before it hits the bottom of the chamber. This allows to avoid the rupture of the mirror and, by lifting it back up, to restart the measurement.

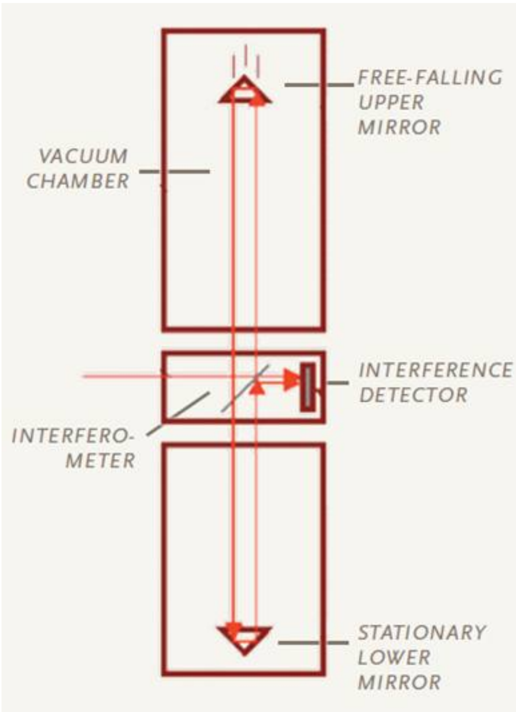

Figure 1.1: Schematics of the FG5-X ballistic gravimeter (Source: Micro-g LaCoste [7]).

The FG5-X has a sensitivity of 15 $\mu\text{Gal}/\sqrt{\text{Hz}}$, comparable to the best available among all kinds of gravimeters in the market to date. However, it is a cumbersome device: it weights 150 kg and occupies 3 square meters of ground floor during operation. This can indeed be inconvenient for a sensor which should normally be transported to obtain data of the gravitational acceleration in different, and possibly hardly accessible locations. We identified the main reason for this bulkiness in the mechanical system used to catch the mirror and lift it back up. The system, in fact, is quite complex, and requires a rapid movement that at the same time avoids the production of mechanical oscillations, which would disturb the gravity measurement. Furthermore, the fact that this system has to be installed inside the vacuum chamber further increases the size of the chamber and the weight of the whole sensor.

As a side note, other kinds of gravimeters perform just as well in terms of sensitivity (in the case of atom interferometry gravimeters, 4.2 $\mu\text{Gal}/\sqrt{\text{Hz}}$ of sensitivity has been reached [8]) and are also comparable in size and weight.

1.3 Project goals

We have seen in the previous section that limitations of current state-of-the-art ballistic gravimeters are mainly centered around the presence of complicated mechanical moving parts, which increase the size and weight of the device. The question arises, whether it is possible to build a new kind of ballistic gravimeter that involves no mechanical moving parts.

This motivation led to the identification of a Paul trap as a possible solution. The idea is in fact to substitute the macroscopic object used in other ballistic gravimeters (most commonly a mirror, like in the FG5-X) with a charged silica nanoparticle levitated in a Paul trap.

A Paul trap is a device consisting of six electrodes, used to trap ions or charged nanoparticles by creating a confining electrical potential [9]. In the approximation of an infinitely-long Paul trap, four electrodes, the radio-frequency (RF) rods, provide confinement in the radial plane of the trap, while the other two, known as "endcaps", provide the confinement in the axial direction. We shall discuss later, in section 1.4, how this infinitely-long approximation affects the trapping potential in the case of a real trap: for now we will use this simplified model in our description.

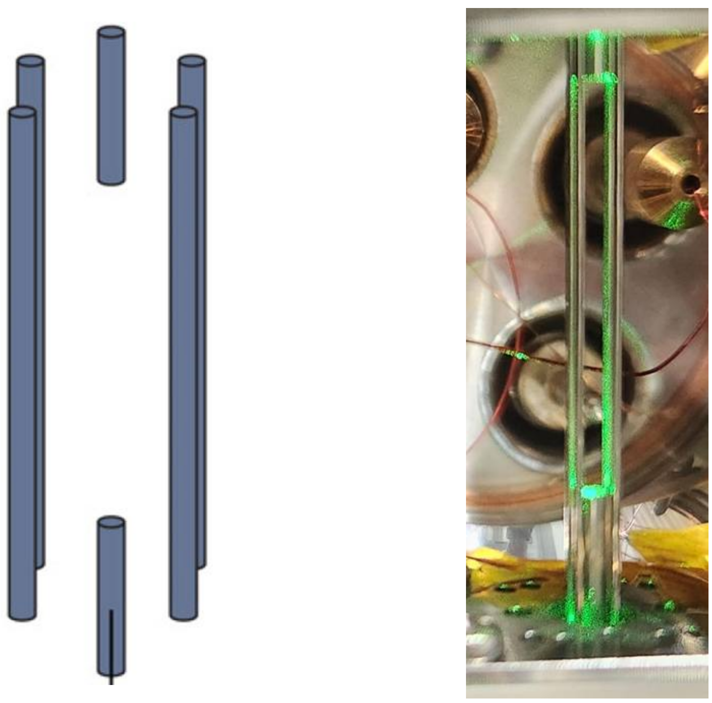

Figure 1.2: Schematic drawing and picture of a Paul trap. The long poles to the sides are the RF electrodes, while the center-top and center-bottom ones are the endcaps. In the picture, the endcaps are separated by about 17 mm.

When a voltage is applied to all the six electrodes (AC voltage on the RF electrodes to confine the particle in the radial plane, and a DC voltage of the same sign of the particle charge on the endcaps to confine it along the axial direction), with equal voltage on the two endcaps, the particle will be confined in the center of the trap. If we align the axial direction of the trap with the direction of the gravitational acceleration, and provided that there is no air friction, when grounding the endcap electrodes, i.e. releasing the axial confinement, we expect the particle to fall due to the gravitational pull. The particle could be then caught in-flight and brought back to the original position by just tuning the endcap voltages of the trap. The position of the particle during the fall could easily be detected using a laser shined on the particle and collecting the scattered radiation, as done in many previous experiments [10][11][12].

The advantages of such an idea, if feasible, should be now clear: no cumbersome or complicated mechanical systems to catch and lift back the falling mass are here required: the confinement and lifting back of the nanoparticle is all done by just tuning voltages. Considering also the size of the Paul trap, which does not usually exceed the few-cm, the vacuum chamber could also be way smaller compared to other ballistic gravimeters (for instance the FG5-X), reducing the size and weight of the whole sensor and allowing for an easier portability. In addition, no complicated adjustments and calibrations to reduce mechanical oscillations generated by the machine itself are required.

With this idea in mind, the goals of the project became therefore:

1. Realize a prototype of such a Paul-trap based ballistic gravimeter.
2. Understand its feasibility and possible limits to the sensitivity.

1.4 First experiment with an existing Paul trap

We therefore initially decided to test the feasibility of our measurement scheme on an existing Paul trap in the Photonics Laboratory of ETH Zurich [13].

We used a Paul trap, with a distance between the two endcaps around 1 cm, to trap a silica nanoparticle. A 532 nm laser was used to illuminate the particle, and a camera was used to collect the light scattered by the particle. The axis of the Paul trap was aligned with the direction of the gravitational acceleration. An image of this setup can be seen in Figure 1.3.

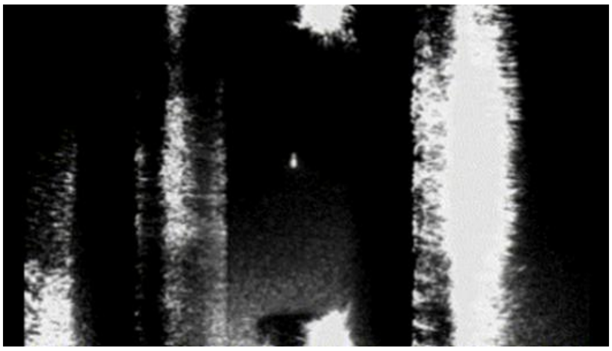

Figure 1.3: Image illustrating the charged nanoparticle (the white dot near the center of the image) trapped in the Paul trap used for the first experimental proof of concept. On the center-top and center-bottom the endcaps can be seen, illuminated by the laser and at about 1 cm from each other, while the vertical bars on the side are the RF electrodes. The direction of the gravitational acceleration is the same of the Paul trap axis, and is pointing downwards.

1. Introduction

To trap the positively-charged particle, the same positive DC voltage was applied to both the endcaps. When we grounded the endcap voltages, to test the falling of the particle, we observed an unexpected behavior: the particle did not fall, but, instead, rose by about 0.05 cm.

We attributed this result to the presence of electric fields along the axis of the trap. We identified three main sources of fields along the axial direction:

1. The RF electrodes, which were not grounded in order to maintain the confinement of the particle in the radial plane. The fact that the Paul trap length is finite causes fields originating from the RF rods to not lay only in the plane (as one would expect for infinitely long metal rods) but to bend in the axial direction.
2. Residual charges in the Paul trap dielectric frame.
3. External stray fields.

This first result directly pointed at the necessity of designing and using a new Paul trap with the goal of minimizing all these sources of axial fields, in order to achieve a free-falling mass along the gravitational acceleration direction. The design of the new Paul trap will be illustrated in detail at the beginning of the next chapter.

Chapter 2

System Overview

The mechanical design of the Paul trap is closely connected to the measurement scheme and size of vacuum chamber. Therefore in section 2.1, we first tried to envision the whole system setup and then introduce the design ideas of the Paul trap. Following the order of things we took in doing this project, we put the COMSOL simulation in section 2.1.1, following by a side notes of assembling the Paul trap in vacuum system in section 2.1.2 and an introduction to the optical setup in section 2.1.3. In session 2.2, we are going to briefly introduce the electronics we need to trap a particle and how we get it. In session 2.3, we describe in detail the vacuum system we chose and the way we load the particle inside the trap.

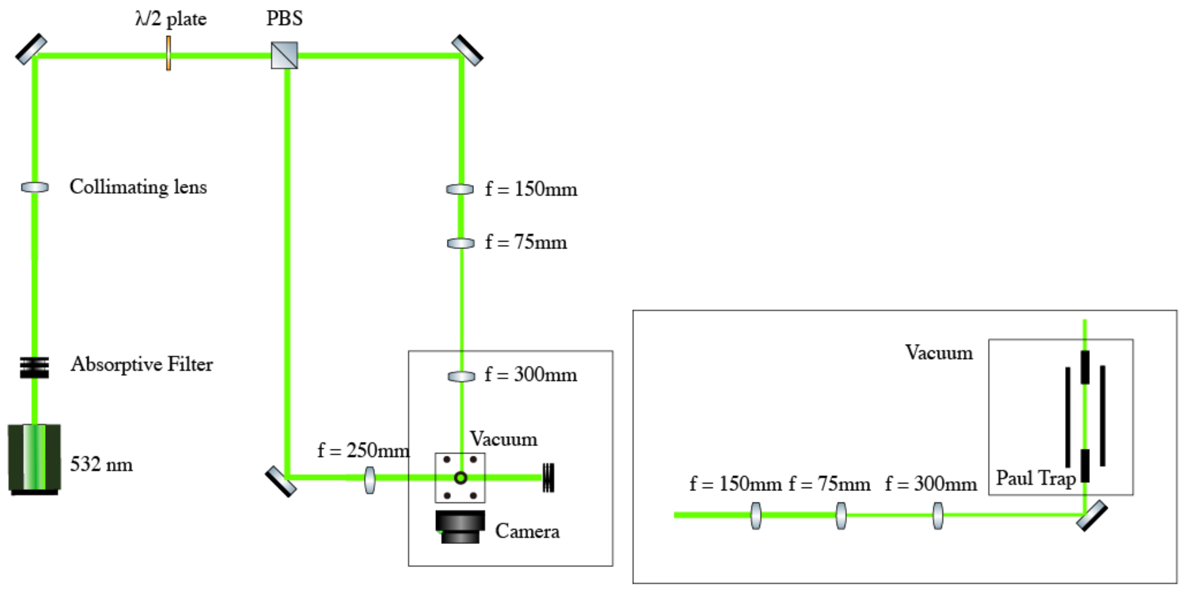

Figure 2.1: System Overview with optical setup, a vacuum chamber and a Paul trap. The 532 nm green laser illuminates the trap in horizontal and vertical direction. The trap is inside a 2.5 inches vacuum cube. A camera observes the trap through the view port of the vacuum chamber. RF and DC signal are connected to the trap by a feedthrough port on the chamber. The detailed connection way can be found in section 2.3.

2.1 Design of Paul trap

The Paul trap based gravimeter includes a Paul trap, two Rf generator, two endcaps voltage supplier, a vacuum system, an optical system, particle loading system and a camera. As depicted in Fig.2.1, the laser illuminates the Paul trap in a vacuum chamber, where the particles can be loaded and trapped when the RF voltage and end cap voltage are on. Tuneable voltage can change the particles position which can be tracked by a camera. Measurement of a gravity is simply data analysis work of the falling trajectory.

The setup here is conceptually similar to the experiment setup mentioned in previous section except the illumination direction. There are two laser beams that respectively shine vertically and horizontally through the trap to light the particle in Fig.2.1, while the other setup only has the horizontally one.

As we learn from the first experiment, The ideal Paul trap based gravimeter should be long enough to reduce the axial field contributed by the RF electrodes and inert enough to resist the influence from the residual charges and external stray field. However, a long trap is worse for detection of particles in this design because it is harder to make a wide enough laser that shine the particles all the way it falls for camera to see. The horizontal illumination of the first experiment setup can only light up a small fraction of a fall according to the size of the beam, which is not desirable.

This motivates us to design the vertical illumination shown separately in Fig.2.1. We use a tube instead of a rod as the bottom and top endcap to let the laser travel through the trap vertically. The geometry of endcap we choose is simply a cylindrical tube, like a metal straw. We choose inner radius and outer radius of the tube to be 0.6 mm and 0.75 mm, which is small enough for laser light to pass through. If a vertical laser beam is well aligned to pass through the small hole of two tubes, we will naturally create a illuminated region along the axis in the trap, in which the particles would be trapped. The particles can always be seen when it falls provided that light intensity is strong enough, no matter how long the dropping distance is.

Although the maximum length of trap set by optical alignment can be more than 20 cm(one can calculate Rayleigh length of the gassuian laser beam as the limits), we choose the length of the trap to be 30 mm. This is because we aim for a compact design that is compatible with a 2.75" vacuum cube. To protect the Paul trap from the stray field, we add shielding plates together with shielding rods. They can be seen in Figure.2.2a: the center part made up of six rods are the Paul trap and all the rest (rods,plates) work to shield. Remember that the simplest Paul trap only have 4 RF rods and two endcaps. The shielding plates and rods are effectively a Faraday cage that enclose the trap inside, which protects the influence of outside field. The distance between RF rods are important for the design of the Rf and DC electrodes of the trap because it determine the trapping volume. To make the trap as ideal as possible, we select the center-to-center distance between neighbour RF electrodes to be 2 mm and the diagonal distance to be 2.828 mm (the four RF electrodes form a square). The length of the trap is 10 times larger than the rods-to-rods distance, which should significantly eliminate the axial field. The lower left corner of fig.A.2a shows a big hole closely surrounded by eight holes and loosely by twelve holes. The outer holes has a rectangular shape. Eight holes locating around the vertex of it are the shielding rods. The edge-to-edge distance between each group is 8 mm, small enough to shield the field and big enough to not block the light.

Versatility is the design highlight of this Paul trap. Instead of using the rods as shielding purpose, we can use them as extra electrodes to influence the field inside RF electrodes. Those shielding rods can be used to compensate the field in three direction, which can reduce the axial field felt by the trapped particles in certain region of the trap. We investigated the characteristic

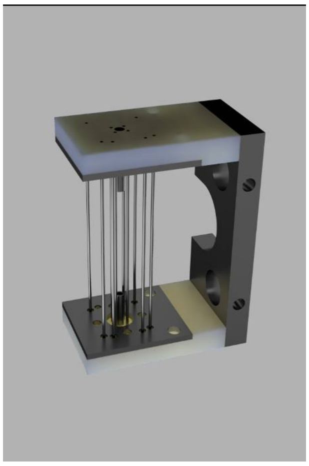

(a) Paul trap. The original Paul trap with four RF electrode and two endcaps is surrounded by eight shield rods and two shielding plates. The dimension of the trap is 30*2*2 mm, while the whole trap is 38*24*16 mm The rods distance of the trap are 2 mm for RF electrodes, 0.414 mm from endcaps to RF electrodes.

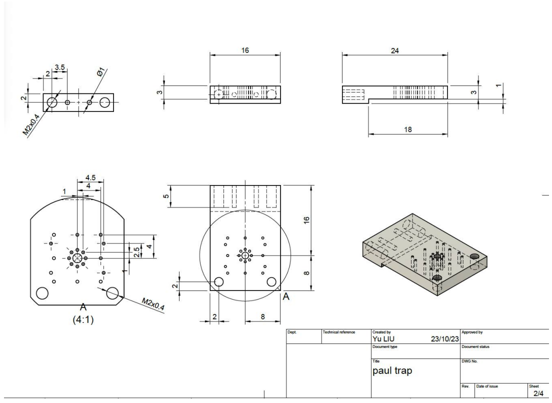

(b) The draft of the supporting frame of Paul tarp. The dimension is 4*16*38mm.Two holes of dimension 6mm to fit the vacuum rods from Thorlabs. Four M2 holes for the screw to connect the shielding plate. Detailed value can be found in the appendix.

of Paul trap setup with Faraday cage in this project. The possibility for other different usage of rods in Paul trap is left for future investigation.

The draft that attached in the appendix was sent to the ETH physics workshop, where the Paul trap was manufactured. One of the drafts is shown in Fig.A.2a for illustration, the other can be found in the appendix. The trap is 38x24x16 mm and made up of 5 components(side support frame, up and down plastic rods holder, up and down metal shielding plate) as frame, 12 rods (8 shielding, 4 RF electrodes) and 2 tubes(endcaps). The assembled Paul trap with all the components mentioned above is shown in Fig.2.2a. The components are fasten by screws, which means it by its own doesn't have mechanical degree of freedom, which is inconvenient for aligning the laser beam. Therefore one can introduce degree of freedom on the device that fix the trap inside vacuum chamber. In our experiment, we introduce one rotating freedom and one translation freedom by groove grabber that can rotate around the axis of vacuum port and an extendable fixing rods that the trap can slide in. Those device are common vacuum components sold by different vacuum system producer . In Appendix A.1, you can find the details parameter and methods we use to design and turn the trap position.

2.1.1 Comsol simulation of Paul trap

We perform a pseudopotential approach to estimate the RF axial fields in the centre of the Paul trap. By directly plugging in the CAD design into Comsol for electric fields simulation, we aimed as well at verifying the theoretical performance of our design. Notice that in simulation, some specific parameters of particle and voltages and a difference in geometry (distance between endcaps) are different from practical setup, and the setup in simulation is shown in Appendix A.2. To put it simple, when only considering fields generated by RF rods, we approximate the pseudopotential of nanoparticle in the radial centre along axial direction by

$$V_{\text{eff}}(z) = \frac{1}{4m}(\frac{n_e e}{\Omega_{rf}})^2 |E(z)|^2$$

[14], with m mass of the particle, n_e charge of the particle, e elementary charge, Ω_{rf} the RF frequency, $E(z)$ spatially dependent electric field amplitude, which could be extracted from Comsol DC simulation, and z the position along the axial direction in the radial centre of the Paul trap. We get the equivalent acceleration of the axial field in AC real case by doing derivative to this potential in z.

$$a_z(z) = -\frac{1}{m}\frac{dV_{eff}(z)}{dz}$$

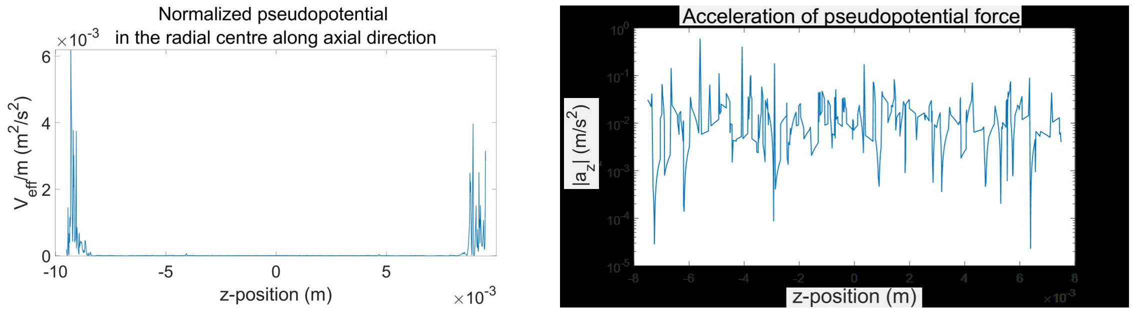

Figure 2.3: Left: V_{eff}/m over z-position extracted from Comsol. We could observe a 1.5cm length of flat zone, where there should be minimized gradient of potential, i.e. RF axial fields.
Right: $|a_z|$ by doing derivative to the left figure in z after smoothing in Comsol.

We observe a long flat zone of pseudopotential of ca. 15mm from the left figure in Fig. 2.3, which indicates that our design should enable a longer falling distance. However, the figure on the right showing absolute value of acceleration at around $10^{-2}m/s^2$ is considered not so credible, because we got too limited amount of datapoints of pseudopotential and thus were not able to determine precise derivative of it. Instead, we got a lot of noisy results due to insufficient sampling, and the right figure shows these results after doing smoothing. Detailed the implementation of simulation and discussion about this problem are elaborated in Appendix A.2.

2.1.2 Assembling of the Paul trap in vacuum system

The hardest part of assembling of the Paul trap is the electric connection between the rods and vacuum feedthrough. The vacuum feedthough is a pin-like connector that connect to a BNC cable outside. In our setup, we need to solder vacuum compatible wires on tiny rods and guide the wires to the feed-through on vacuum system. Any contact between the wires forms essentially a high pass capacitor. If one AC wires contact with a DC one, this effectively connect the high frequency AC signal to the ground, which distorts the output waveform significantly. To avoid such effect, we carefully route the wires in a small vacuum chamber with vacuum tapes to separate them. We suggest to install the feedthough port at the very last stage and focus on sorting the wire at the beginning, because installation of wire inside vacuum chamber could be tedious.

2.1.3 Optical setup

As is drawn in Figure 2.1, We use a 532 nm wavelength laser with power 300 mW as our laser source, a half wave-plate to select the polarization and tune the laser power, a beamspliter to separate horizontal and vertical illumination. A telescope shrinks the beam to pass it through the holes on the caps with two lens to alter the direction and position of laser beam.

The vertical alignment of Paul trap is achieved by a spirit level putting next to the trap. We try to ensure that the trap parallel with the spirit level when installing and then align the two lens of laser beam to let the light pass through. In our setup, the alignment is tricky but we didn't find precision of alignment as a limiting factor to fall a particle. Ensuring a laser than pass through both caps are enough.

A careful alignment can deliver 10% of the light power to the vertical illumination path, comparing with the light from the laser device. Most of power is lost on the misalignment of half-wavelength plate with respective to the incoming beam. We use an absorptive filter to reduce the original output laser power from 300 mW to 10 mW. The power of vertical illumination is around 1 mW. It is important to notice that this design is not optimized. Using of simulation software like Zemax should allow better design of optical system.

2.2 Electronic design and characteristic

The electronics we need are the DC and RF voltage suppliers that control the voltage on the rods, which provide electric confinement to the trapped particles. Low voltage like 30 V suffice the use of operation on endcaps. Therefore we use the lab power source. However, trapping of particles requires ±200 V AC signal at 10 kHz on the RF electrodes, which is only a functionality of expensive equipment(more than 10000 CHF). Considering that there are not existing spare device like this in the lab, we chose to build our own electronics that produce high voltage RF signal. We inherited the Print Circuit Board (PCB) design from Gabrielle's thesis[15] and mainly focus on rebuilding and improving the design. It functions as a switch between two high voltage like +500 V and -500V with bandwidth 100kHz, which is enough for our use. This subsection only provides essential information in understanding the circuit. In depth description of the circuit can be found in Appendix A.3.

The circuit design is shown in Fig.A.4. This PCB is powered by +500 V and -500 V DC volatge from a high voltage DC supply F10CT with two MOSFET forming a half bridge converter that can switch between the voltage according to input value to output square wave. The design first uses a optical coupling(6N137M) to move the ground of input signal to virtual voltage(-500 V). Then a Xor gate(SN74LVC1G86DBVT) between the signal and a high or low value(controlled by a mechanical switch) to logically change the phase of waveform(0 or 180 degree). Then, it use a MOSFET(BST82.215) for amplification of the input signal and two MOSFET driving circuit(IR2184 & IR2213) to power up the MOSFET between $\pm 500V$, refering to the input signal. The second MOSFET(IR2213) driving circuit follows the bootstrap circuit to open and close two MOSFET , while the first MOSFET(IR2184) circuit drags the input voltage to $\pm 15V$.

The design requires DC amplifier F10CT to convert 12V input to ± 500 V DC output, a assembled PCB board and an signal generator. We use RIGOL DG812 for signal generation, assemble the PCB ourselves.

On implementing the design, we observed a voltage drop at very low switching frequency(around 100 Hz). Considering that for power electronic, the output voltage drop is closely related to a over consume of energy, we attribute this effect to an energy-inefficient MOSFET. The MOSFET (NTHL020N120SC1) shown in the circuit diagram consumes nearly 10 times more energy(3 mJ/switch) than the one actually used in a working PCB (0.3 mJ/switch) in the lab. To make our PCB work, we replaced the MOSFET with the one used in his design and the circuit works. An equivalent solution is to use AIMW120R060M1H, a low loss MOSFET that works well for

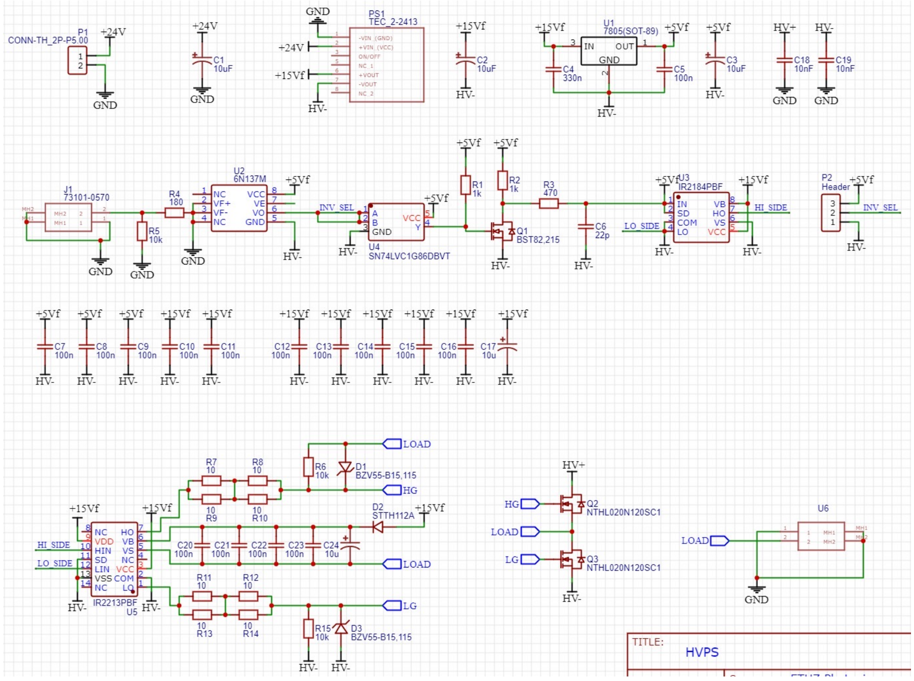

Figure 2.4: The draft of circuit produced by Gabriele in his thesis[15]. We follow his design to produce this PCB. Noted that the transistor NTHL020N120SC1 is not the correct one.

switch between high voltage. Details datasheet can be found by searching the name of MOSFET in different supplier.

2.2.1 Assembling PCB

Soldering the components on the PCB is not trivial. it is important not to overheat the PCB board or it will be tough to solder unless cleaned. Several backup sets of whole components of PCB should be bought in case it breaks. It would be also nice to use a component container on the PCB for easy disassembling. Taking out a chip with eight pins soldered on the PCB with soldering gun usually damages both PCB and chips.

2.3 Vacuum system

For the vacuum chamber we required a trade-off between a compact system and having a large number of access ports. After in depth analysis, we identified the following as unavoidable:

1. One port for the vacuum pump.
2. Electrical feed-through for six BNC cables (two for the two pairs of RF electrodes, two for the independently-controlled endcap electrodes, two for the two pairs of shielding/compensation electrodes). We therefore used two 4-pin BNC feed-through ports.
3. Two windows to be placed in the vertical direction, to have vertical optical access.
4. Two windows in the horizontal plane, one for the horizontal laser to shine through and one for the camera/photodetector.

which accounts for a total of seven ports.

We therefore decided to use a 2.75" cube from Kimball Physics. On top of this, a 2.75" cross was mounted. This gives a total of 6+4−2=8 ports (the "−2" to account for the connection between the cube and the cross) which was enough. We therefore installed one window on the bottom side of the cube, and one on the top of the cross, so to have vertical access along the full cube+cross chamber. On one of the cross arms we placed a 4-pin BNC feed-through port, and on the other one the vacuum pump tube (we used another cross there to allow the installation of a pressure sensor). On the remaining 4 ports of the cube we installed the other 4-pin BNC feed-through and three windows. We chose to have an additional window for higher flexibility on where to send in the laser and position the camera. Figure 2.5 illustrates the vacuum chamber setup.

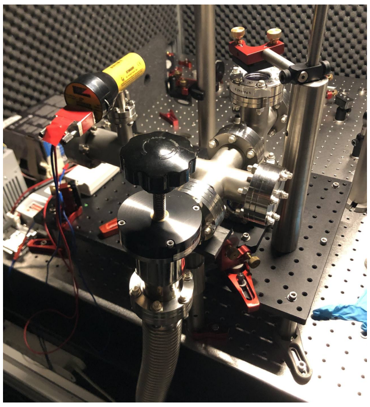

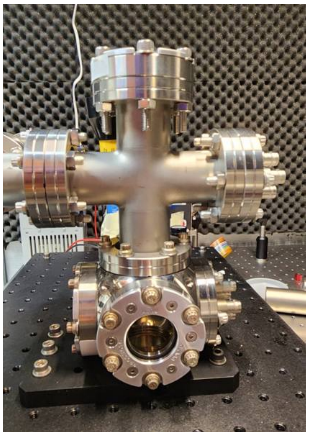

Figure 2.5: Two images from different angles of the vacuum chamber. The yellow tube is the pressure sensor, while the black knob is a vacuum valve. The vacuum pump is positioned under the optical table, at the end of the tube heading downwards in the front of the left picture.

The setup worked and allowed us to reach a pressure of 10^{-4} mbar within minutes from the activation of the pump. However, to point out a couple of drawbacks (and possible directions of improvements) the narrow size of the cube made it at times hard to install the Paul trap inside it and to route the wires from the trap to the BNC feed-through port positioned on the cross. Finally, the absence of a quick access port made it slightly annoying to have to unscrew and screw back a window every time to open the chamber, load new particle and close the chamber (especially considering the particle loss rate during the first dropping experiments, which required frequent loading of new particles).

2.3.1 Particle preparation and loading

There are many ways to load the particle inside the trap including methods like LIAD, electrospary and nebulizer. While LIAD can load the particle in high vacuum, it requires a high power pulse laser, which is inaccessible in our project. We choose electrospray(ESI) technique because it is stabler to load the particle comparing with using nubulizer. Performing Electrospray needs to charge the little droplet of particles solution with high voltage. If we put the liquid to a small metal hollow tube and apply high voltage on the tube, the liquid will be charged and pushed out of the tube like shooting a bullet. The liquid will quick evaporate when it is shot, leaving charged nanoparticles flying. If the particles pass a functioning Paul trap, it can

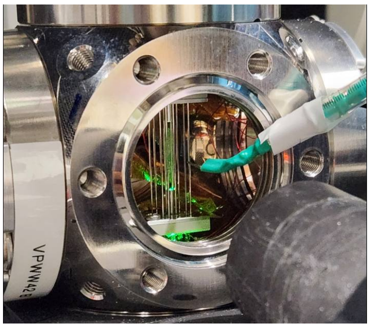

Figure 2.6: Electrospray inside a trap. The green injector contains the solvent of nanoparticle. A high voltage source is connected to the tip of the injector. To load a particle, we push a droplet out of the needle and apply 1200 V on it. The particle will be shot out and some of them can be trapped. With vertical illumination, those particles can be seen.

be captured.

To deploy ESI, we dilute 2 μl 519 nm diameter nanoparticles in 99% isopropanol and put it inside a special made medical injector, which is the common medical used one with the needle connect to the high voltage source. We power up the needle with 1200V by a high voltage generator to charge the needle and put the injector to spray the particle inside the trap. Fig.2.6 shows such operation. The green tape wrap the tip of needle that are charged by 1200V. Pressing the injector will shoot a stream of charged droplets to the open trap. If the particles are trapped, We then seal the vacuum port, open the pump and push the system into vacuum environment.

Chapter 3
Results

Combining all the components mentioned above, we start to trap and manipulate the particles inside our trap. Since we are only interested in making the particles fall with radial confinement, whose precondition is that they are successfully trapped, we didn't conduct full characterization of our Paul trap, i.e. sweeping composition of trapping parameters (RF voltage, RF frequency) and extracting a stability diagram. Instead, We discovered a certain parameter range where trapping is stable based on observation and prior experience.

In order to study the phenomena in low vacuum, where influences from air flow and friction are ruled out, we discovered the protocol to evade plasma which will be elaborated in Section 3.2 when entering into low vacuum, which would cause short circuit and thus loss of all particles. By changing different configurations, we found that with shielding rods and "better" (closer to an ideal infinitely long one) trap geometry, RF axial fields in the center, which are the dominant factor preventing the particle from falling when DC endcaps are turned off, could be significantly reduced from an unknown larger value to the extent that their effect on the particle over the whole trap vertical length is smaller than that of gravity. We extracted the particle trajectory with a tracking software from a video recording the fall, and did some analysis.

However, due to time limitation of this project, we are still limited by the capability of DC electronics and RF axial fields could still be further understood and minimized.

3.1 Trapping of particles

A picture of trapped particles is shown in Fig.3.1. The string of green dots are the trapped particles. They are visible by eyes with illumination of vertical laser of ca. 0.9 mW, and diameters of "green dots“ are larger than particles themselves due to scattering ·In this experiment, we use trapping amplitude ca. 170 V, frequency 10 kHz and 30 V symmetric endcaps voltage. From now on, these parameters would be expressed as (RF voltage, RF frequency, top endcap voltage, bottom endcap voltage) = (ca. 170 V, 10 kHz, 30 V, 30 V).

Though full characterization of trapping parameters wasn't conducted, with both endcap voltages fixed at 30V, we fixed respectively RF voltage and frequency at regular value, and varied another parameter to find its range of stability: When RF voltage is fixed at ca. 300 V, the stable range for RF frequency is 3 kHz to 40 kHz (varied by 1 kHz each time); when RF frequency is fixed at 10 kHz, the stable range for RF voltage is ca. 100 V to 550 V.

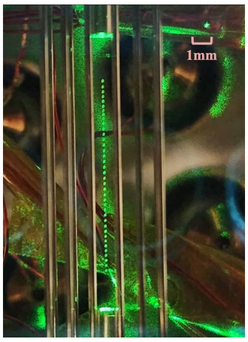

Figure 3.1: Trapping particles. (ca. 170 V, 10 kHz, 30 V, 30 V)

3.2 Protocol towards falling experiments

To observe phenomena and draw valid conclusions, low vacuum is required to rule out the influence from air friction and airflow, and it's also necessary to preserve only one charged particle in the trap so that repulsion between particles wouldn't affect the motion of single particle. Collective motion of multiple particles was not investigated due to limited knowledge about the distribution of complex axial fields.

As mentioned in 2.1.2, contact between wires with high voltages would cause short circuit and thus loss of all trapped particles. Similar things would happen when the system goes closer to low vacuum if RF voltage is too high. Fig.3.2 shows the plasma we encountered when entering into low pressure. The effect is especially strong when the pressure is around 10 mbar, and weaker at lower or higher pressure, and it's caused by the fact that in our Paul trap design, endcap rods and RF rods are too close to each other. By lowering RF voltage we could lower the system pressure "safely" to around 2.5×10^{-3} mbar. The practical protocol of ours is: first trap particles with parameters (ca. 300 V, 7-10 kHz, 30 V, 30 V) at atmosphere; tune the RF voltage down to ca. 150V to evade plasma; turn on the pump till the pressure reached around 2.5×10^{-3} mbar. And at this pressure we could already tune the electric parameters arbitrarily.

And while entering into low vacuum, usually we would lose some particles. To preserve only one in the trap, we took advantage of the tunability of 2 endcap DC sources, unbalanced them to push extra particles upwards or downwards through endcap holes out of the trap. A more common scheme is to tune up RF frequency gradually to destabilize trapped particles and lose extra ones.

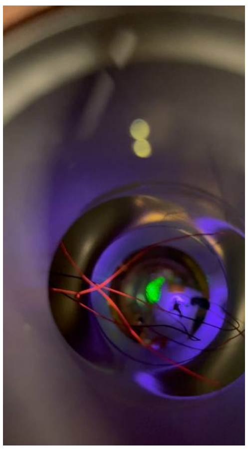

Figure 3.2: Plasma effect observed from top

3.3 Falling experiments

From now on we start to show three representative falling experiment results conducted in low vacuum environment, where the pressure is ca. 2.5×10^{-3} mbar.

3.3.1 A short fall

To verify our improvements to the Paul trap design step by step, we didn't apply shielding rods at first. As indicated in Fig.3.4, with both endcap voltages balanced at 30V, the particle was initialized around centre height in the trap. After switching off 2 endcaps voltages at the meantime, we observed a fall of only ca. 0.4 mm.

We identified potential problems as below:

1. External stray fields: we hadn't applied 8 shielding rods yet.
2. Misalignment of the Paul trap: it was hard to align the trap perfectly to the gravitational direction, since we could only manually fix the groove grabber holding the trap frame onto the chamber port and adjust the angle. The particle could have fallen deviated from centre, thus enduring larger RF fields.
3. RF axial fields: RF rods still generated axial fields in the centre.

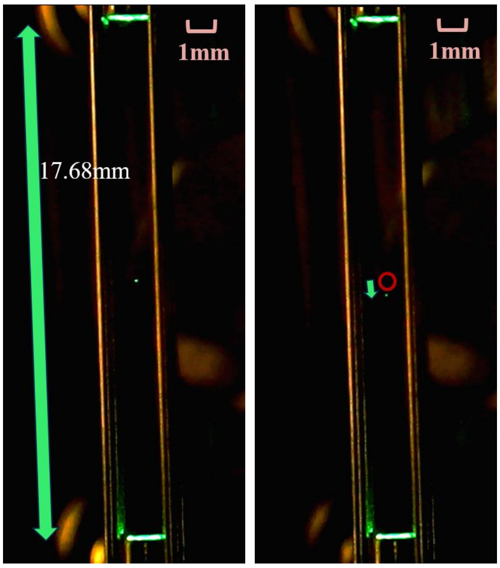

Figure 3.3: A short fall of trapped particle (the little green dot in the centre) in the first series of experiments. The vertical distance between 2 endcaps is 17.68 mm.Trapping parameters are (ca. 170 V, 10 kHz, 30 V, 30 V) in the beginning as indicated on the left. The figure on the right shows fall of the particle after switching off 2 endcaps DC voltages to ground (ca. 170 V, 10 kHz, 0 V, 0 V). The red circle labels the initial position and the green arrow labels the length of the fall, ca. 0.4 mm.

3.3.2 A fall with unbalanced endcap voltages

After spotting the potential problems from our first falling experiment, we applied those shielding rods, as indicated in the image to shield our system from external stray fields. And we also did a re-alignment of the whole Paul trap to the gravitational direction.

This time the particle was initialized and stayed above center even with unbalanced endcap voltages (top endcap +70 V, bottom endcap -30 V) that were actually trying to pull the particle down. As we slowly tuned up the top endcap voltage from 70 V, the particle slowly and only slightly (much smaller than 0.1mm) moved downwards.

When it reached 80V, we observed that the particle suddenly fell for ca. 0.7 mm. We consider this as a proof of the existence of unevenly distributed RF axial fields, which still dominated over gravity overall, but much smaller in some certain region where the particle fell, which is a good sign. We have the hypothesis that there could exist multiple local minimums of pseudopotential created by RF rods. This explains phenomena that particles were trapped stably at these two points but able to fall between them, and that the particle barely moved when we tried to tune up the RF frequency (which would decrease all RF fields, including the axial fields in the radial centre, based on the theory of pseudopotential).

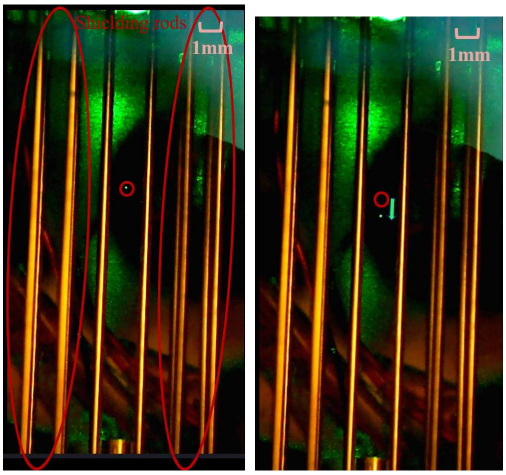

Figure 3.4: A sudden fall of trapped particle (the little green dot in the centre) when slowly tuning up the top endcap voltage. The vertical distance between 2 endcaps is still 17.68 mm and the circled rods are shielding rods applied in this experiment. Trapping parameters are (ca. 170 V, 10 kHz, 70 V, -30 V) in the beginning as indicated on the left. The figure on the right shows fall of the particle after the top endcap voltage reaches 80 V. The red circle labels the initial position and the green arrow labels the length of the fall, ca. 0.7 mm.

3.3.3 A full-length fall

We tried to reduce RF axial fields in two respects:

1. Enlarge the distance between two endcaps from 17.68 mm to 19.80 mm: this could be seen as that we optimized our Paul trap geometry closer to an infinitely long one, in which ideal case there would be no RF axial fields in the radial centre.

2. Reduce number of charges on the nanoparticle by decreasing the voltage used in electrospray: so that all electric forces were reduced by a factor.

The particle was initialized above center with top endcap grounded and bottom to 100 V, then we suddenly switched off the bottom and observed a fall of almost the whole vertical region.

ca. 14.0 mm. This means we managed to suppress the impact from all of the fields and forces that were hard to control to lower than the impact from gravity. When looking at the original real-time video, it looks like the particle was experiencing a free fall. However, a closer analysis of the video with the assistance of tracking software in the following subsection could tell us the fall wasn't a free one and the particle motion was more intricate.

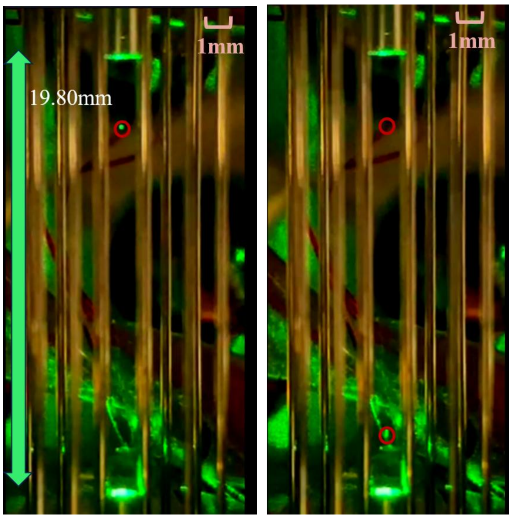

Figure 3.5: A full-length fall of trapped particle (the little green dot in the centre) when switching off both endcap voltages. The vertical distance between 2 endcaps is now 19.80 mm. Trapping parameters are (ca. 230 V, 20 kHz, 0 V, 100 V) in the beginning as indicated on the left. The figure on the right shows fall of the particle after switching off the bottom endcap voltage also to ground, i.e. 100 V to 0 V. The red circles label the initial and final positions and the length of the fall is ca. 14.0 mm.

3.3.4 Analysis of full-length falls

To analyze the motion of the particle we used "Tracker: video analysis and modelling tool" [16]. The precision of this method was limited by the pixel resolution of the camera and, more importantly, by the limited amount of frames per second. However, it is a quick measurement setup to implement and characterize the fall, when no particular precision is required yet. And we use data from different stages of multiple full-length falls, for part of the falls are untraceable due to the disturbance from background light.

First we tracked the position of the particle during the fall. Figure 3.6 shows the falling length over time in the first length of a full-length fall.

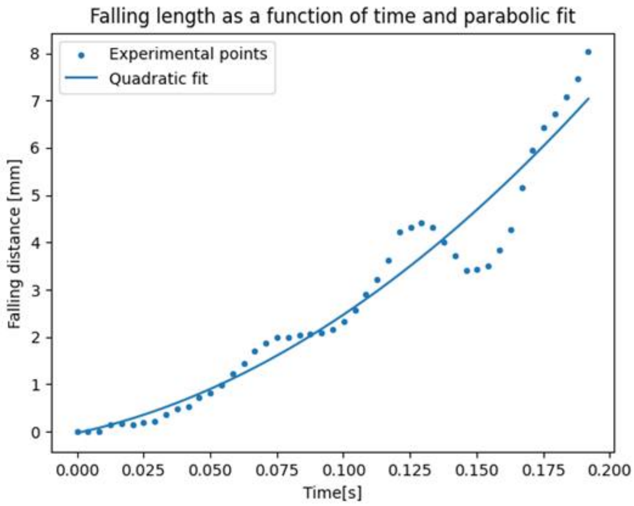

Figure 3.6: Particle falling length over time and a quadratic fit in the first half length of a fall.

It can be clearly seen that it is not a free fall, as the particle, after $0.125s$ after starting to fall, rises shortly. In fact, the acceleration value extracted from the quadratic fit is only 0.24 m/s^2.

Looking back at the protocol, we spotted a problem in switching off the endcap. Fig 3.7 shows the response curve of it. It takes 176ms for it to completely switch off, so nearly in the whole range of the trajectory shown in Figure 3.6, the particle experiences the upward DC electric force generated by the bottom endcap. This could be part of the reasons why the acceleration a is so much smaller than g.

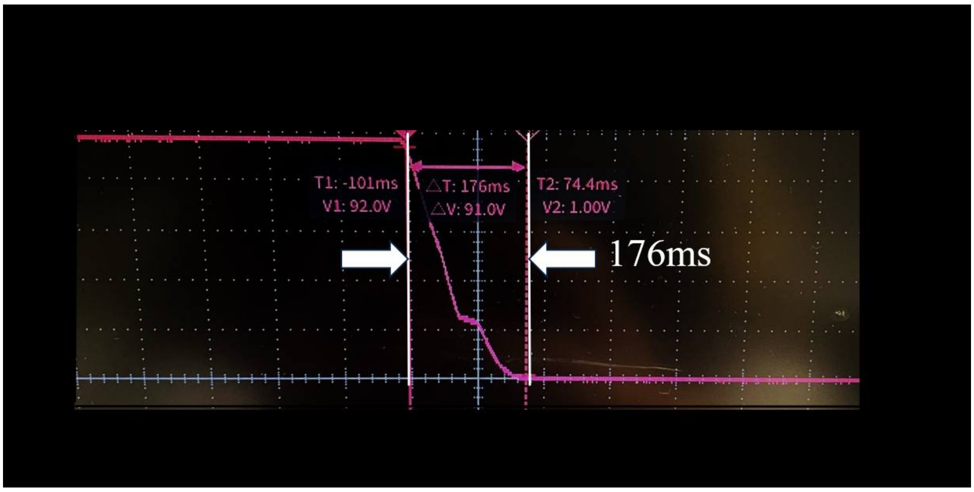

Figure 3.7: Response curve of switching off bottom endcap voltage. The graph was extracted by directly connecting the oscilloscope to the DC voltage source set at 100V and suddenly turning it off.

We then moved to analyzing the damped oscillatory motion that the particle exhibits at the end of the fall (which couldn't be found in Figure 3.6 due to technical issues). We first want to draw attention here on the fact that we did not turn the endcap voltages back on at the end of the fall: the axial fields far from the center of the trap are strong enough to trap the particle. This is an unavoidable effect that we expected from simulations, and it would not be a problem for the sensor as the free-fall of the particle could be considered only around the trap center. That being said, the damped oscillatory motion is caused by the accumulated kinetic energy being slowly dissipated by the air friction while the particle is trapped at the end of the fall. Figure 3.8 left shows part of damping oscillation during the last stage of a fall and right shows the decreasing amplitude with time and exponential decay fit. The exponential fit returns a damping coefficient γ =0.87 Hz, in good agreement (within a factor 2) with the calculated value from the theory [11]:

$$\Gamma_0 = \frac{6\pi\eta R}{m}\frac{0.619}{0.619 + Kn}(1 + c_K)$$

, where we plug in particle radius R, mass m, η corresponding air viscosity at pressure of $2.5 \times 10^{-3} mbar$, Kn Knudsen number and c_k dependent only on Kn, and get a theoretical approximation of ca. $0.4Hz$.

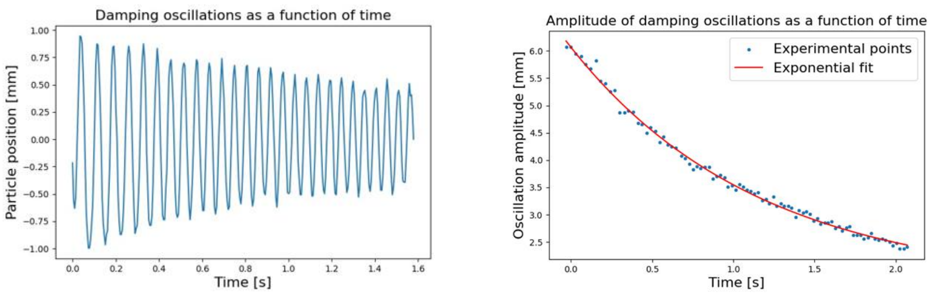

Figure 3.8: Left: Part of the particle trajectory of damping oscillation during the last stage of another fall (different from the previous one).
Right: Experimental points of oscillatory motion amplitude and exponential fit.

Besides electric fields and air damping, the vertical laser for illumination also applies radiation pressure on the nanoparticle, which we have to take into account and estimate. We calculated the scattering cross section of our 519nm SiO_2 nanoparticle based on Mie scattering theory with existing Matlab code [17] to be $C_{scs} = 2.4132 \times 10^{-12} m^2$. With an estimation of the upper limit of laser intensity

$$I = \frac{P}{\frac{1}{2}\pi w_0^2}$$

, we assume the whole particle is in the centre of Gaussian beam. $P \approx 0.9mW$ and $w_0 \approx 0.6mm$ are respectively beam power and beam waist of the vertical laser in experiments. And the acceleration induced by radiation pressure is

$$a_{scs} = \frac{IC_{scs}n_m}{mc} = 7.93 \times 10^{-2} m/s^2$$

, where $n_m \approx 1$ is the relative refractive index in low vacuum, c velocity of light and m mass of the particle. The acceleration value is much smaller than g, which means radiation pressure wouldn't cause obvious influence to the particle motion, but it could be relevant after we rule out other dominant factors, acquire a nearly free fall of the particle and a precise measurement of g.

Chapter 4

Conclusion and Outlook

Gravitational acceleration measurement is important in a wide range of applications. A compact and cheap gravimeter finds its advantages in geological exploration, mineral detection. In this project, we developed prototype of a new type of compact and cheap gravimeter: Paul trap based ballistic gravimeter. Our idea originates from the typical interferometric ballistic gravimeter(FG5-X), where the gravitational acceleration is extracted from the trajectory of a falling mirror recorded by an interferometer. We propose a new type of gravimeter using nanoparticle instead of mirror to repeat the falling process and camera instead of interferometer to track the falling. Using Paul trap to control the position of particle and let it fall, we can avoid mechanical disturbance to the falling object and thus reach a very compact design. The ideal sensitivity could be comparable with the interferometric ballistic gravimeter, as you may find in the appendix. The technical difficulties arises from the axial field induced by finite side effect and charge accumulation of a linear Paul trap. As we found in a Paul trap in the lab, the gravity doesn't overcome electric force in the center even when we removed the axial electric confinement introduced by two endcap.

To eliminate the field, we designed and built a new linear Paul trap with longer length of 3 cm and shielding plates and rods. In order to test the new Paul trap and get some measurement result of gravity, we set up the whole system for the ballistic gravimeter with following metrics: optical system that can vertically illuminate the trap with at least 0.1 mW in power, RF generator that output $\pm$ 500 V RF signal, a vacuum system that goes to 10^{-3} mbar. We built a optical system using telescope to allow 10% power of light to pass the pin hole of two endcaps vertically, which light up the place that particles could be trapped. We manufactured a cheap RF generator PCB to generate high voltage square wave with bandwidth 120 kHz and output absolute voltage 500V. We tested the vacuum chamber without trap installed and found it reach 10^{-4} mbar.

With the components mentioned above, we successfully trapped the Electrode-spray loaded particles using RF voltage 300V, frequency 7 kHz, two endcaps with +30 voltage. With a single particle trapped, our experiment procedure works as following: initialize its position near the top endcap, turn off both endcap to let gravity drag the particle, use a camera to record this falling and calculate the gravitational acceleration. We initially observed a tiny falling of sever millimeter on an asymmetric endcap and no-sheilding Paul trap. After we tuning the endcaps length, adding shielding component to the trap and reducing the charge-to-mass ratio of the particles, we obtained a long fall with ca. 14 mm. Although there are still local potential minimums that modulate the particle, we conclude that the gravity dominates the falling process. The particle oscillates strongly at the end of the falling, whose damping ratio is comparable to a harmonic oscillator at the same vacuum level. This indicates the absent of axial field in the oscillating region.

After our very first step towards a ballistic gravimeter based on Paul trap, making the particle fall for a long distance with RF radial confinement in the Paul trap, during which gravity dominates over all other forces, further steps and possible improvements could still be done:

1. Further understand and minimize RF axial fields

   (a) by tuning down RF voltage or tuning up RF frequency as long as the particle can still be trapped;

   (b) by enlarging the distance between endcaps or possibly by using the two metal plates (currently used for shielding in the vertical direction) as endcaps instead of currently used tube rods.

   Notice that with the former approach fields are reduced by a factor just like reducing charges on nanoparticles, while with the latter Paul trap geometry and distribution of electric fields are optimized. The latter is considered as more promising from our perspective if we aim at a good gravity sensor with high sensitivity, since improvement from the former is always limited by capability to trap. And with plates as endcaps, it's possible that we would have larger vertical space around trap centre where RF axial fields are minimized, since they are farther from the centre and flatter compared to tube rods. Higher tunable DC sources would be needed for plate endcaps to move and levitate the particle.

2. Build a control system with better electronics to automate repetitive falling and levitating mechanism:
   With fast electronics and control system we would be able to switch off/ back on the DC endcap voltages quickly enough such that the particle motion wouldn't be disturbed as in our case where it's done purely manually. In fact, even without control system, having fast electronics would be enough to examine the particle motion affected only by RF axial fields, gravity and air damping for the current setup and as well as how long a nearly free falling (RF axial fields small enough) vertical range there exists around the centre of the Paul trap. Moreover, automated repetition of the mechanism would gain a higher sensitivity over a period of measurements in the future.

3. Implement a measurement scheme:
   A precise measurement scheme is necessary for a gravity sensor, and the design of vertical optical access allows for different detection schemes, among which backward detection is recommended for a higher detection efficiency.[18]

4. Implement an initialization system to approach Standard Quantum Limit (SQL) of free-fall gravimeter:
   The ultimate goal for this project, is to pursue a perfect Paul trap, in which the particle could do free-fall meanwhile with radial confinement from RF fields, such that we have a free mass in the gravitational direction. With the ballistic regime, we would need a good initialization system (e.g. another optical trapping and feedback cooling system) to enter into quantum regime, thus approaching SQL. Detailed calculation and discussion written by Dr. Martin Frimmer can be found in Appendix.

Bibliography

[1] T.A Herring. *Geodesy: An introduction and Overview.* Treatise on Geophysics - Editor-in-Chief: Gerald Schubert, 2015.

[2] L. Timmen. *Absolute and Relative Gravimetry.* Xu, G. (eds) Sciences of Geodesy - I. Springer, Berlin, Heidelberg, 2010. URL: https://doi.org/10.1007/978-3-642-11741-1_1.

[3] Jiaqi Zhong, Biao Tang, Xi chen, and Lin Zhou. "Quantum gravimetry going toward real applications". In: *The innovation 3(3), 100230* (2022).

[4] G. M. Tino and M. A. Kasevich. *Atom Interferometry.* Societa Italiana di Fisica and IOS Press, 2014.

[5] D. K. Shaeffer. "MEMS inertial sensors: A tutorial overview". In: *IEEE Communications Magazine, vol. 51, no. 4, pp. 100-109* (2013).

[6] L. F. Vitushkin. "Absolute Ballistic Gravimeters". In: *Giroskopiya i Navigatsiya, 2015, No. 3, pp. 3–12* (2015).

[7] URL: https://microglacoste.com/product/fg5-x-absolute-gravimeter.

[8] Zhong-Kun Hu, Bu-Liang Sun, Xiao-Chun Duan, Min-Kang Zhou, Le-Le Chen, Su Zhan, Qiao-Zhen Zhang, and Jun Luo. "Demonstration of an ultrahigh-sensitivity atom-interferometry absolute gravimeter". In: *Phys. Rev. A 88, 043610* (2013).

[9] Paul W. and Steinwedel H. "Ein neues Massenspektrometer ohne Magnetfeld." In: *RZeitschrift für Naturforschung A 8 (7): 448-450* (1953).

[10] T. M. Ostermayr, J. Gebhard, D. Haffa, and et al. "A transportable Paul-trap for levitation and accurate positioning of micron-scale particles in vacuum for laser-plasma experiments". In: *Rev. Sci. Instrum. 89, 013302* (2018).

[11] Jan Gieseler, Bradley Deutsch, Romain Quidant, and Lukas Novotny. "Subkelvin Parametric Feedback Cooling of a Laser-Trapped Nanoparticle". In: *PRL 109, 103603* (2012).

[12] Tebbenjohanns Felix, Frimmer Martin, Militaru Andrei, Jain Vijay, and Novotny Lukas. "Cold Damping of an Optically Levitated Nanoparticle to Microkelvin Temperatures". In: *Physical Review Letters 122, 223601* (2019).

[13] Tobias Zwahlen. *LIAD Loading.* Master. 2023.

[14] D. Kienzler. *Trapped-ion Physics Lecture.* 2023.

[15] Gabriele Johannes Giuli. "Towards Spin Control of NV- Centers in Levitated Diamond Nanocrystals". Thesis. 2022.

[16] URL: https://tracker.physlets.org/.

[17] Andrea Baldi. *Mie Scattering and Absorption Sphere.* https://github.com/andrea-baldi/Mie_Scattering_and_Absorption_Sphere/releases/tag/v1.0.2. GitHub. 2024.

[18] Felix Tebbenjohanns, Martin Frimmer, and Lukas Novotny. "Optimal position detection of a dipolar scatterer in a focused field". In: *Phys. Rev. A* 100 (4 Oct. 2019), p. 043821. DOI: 10.1103/PhysRevA.100.043821. URL: https://link.aps.org/doi/10.1103/PhysRevA.100.043821.

Appendix A

Engineering material

A.1 Design of Paul trap

Figure A.1 and Figure A.2 shows the draft of the supporting frame. Two dielectric supporting plate are screwed on two ends of the metal support. The two big holes in the metal frame will hold the rods, which is grabbed by a groove grabber on vacuum port. Two screws on the side of the metal support fix the rods. Therefore, the trap position is set. The shielding plate are screwed with two M2 screw on the supporting plate.

The small holes on the plate are capable for 0.5 mm diameter rods. The RF rods must be larger than 38 mm to be fully installed. Extra 5 mm length is left for soldering the rods.

On shielding plate, we use radius of 0.6 mm and 0.75 mm holes for electrodes to pass through to ensure that there aren't big capacitor forming. We insert four electrodes in diagonal position to have better visibility from the side.

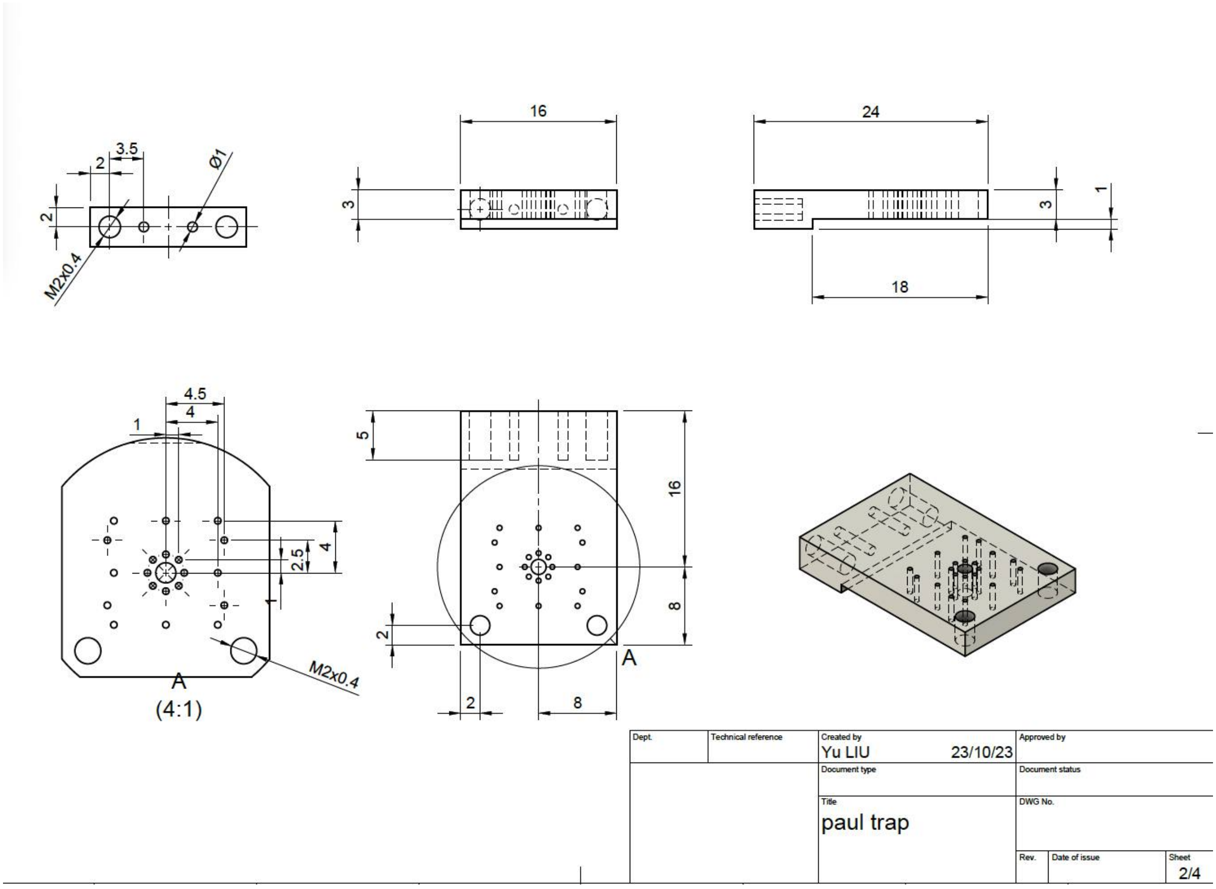

Figure A.1: The draft of the dielectric supporting plate of the Paul trap. The trap geometry is defined by the position of holes on the plate. The holes diameter are 0.5 mm and 1.5 mm. M2*4 screw is used to install the shielding plate.

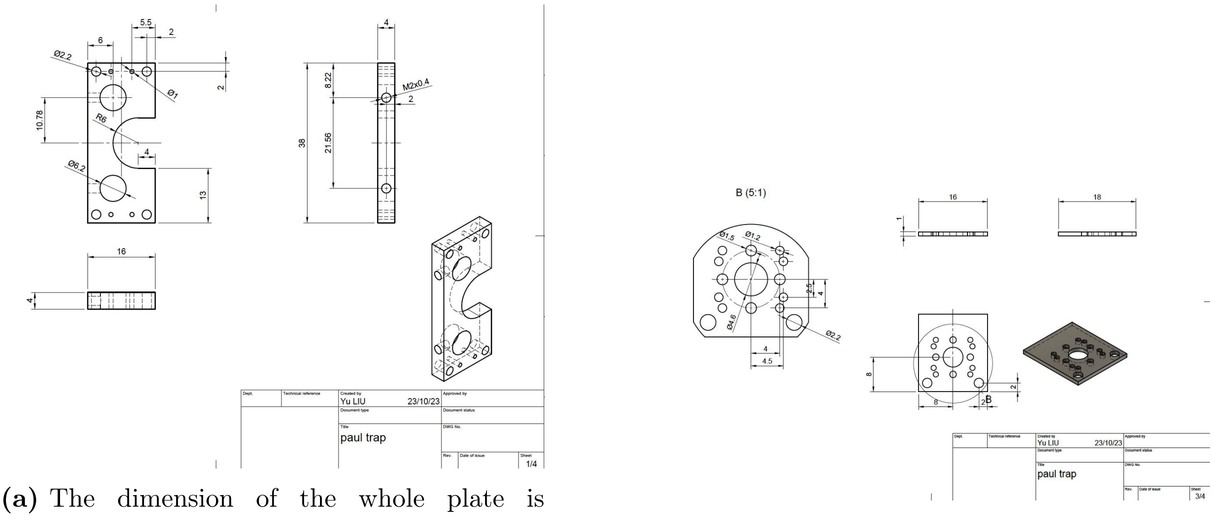

(a) The dimension of the whole plate is 4*16*38 mm.Two holes of dimension 6mm to fit the vacuum rods from Thorlabs. Four M2 holes for the screw to connect the shielding plate.

(b) The dimension is 16*18*1 mm. For every position of the rods, there is a larger radius hole to avoid forming of large capacitor.

Figure A.2: The draft of metal supporting plate and metal shielding plate of the Paul trap. (a)The metal support frame to connect the trap with vacuum chamber.(b)The dielectric shielding plate.

A.2 Comsol simulation

As mentioned in 2.1.1, we plugged in the CAD design of Paul trap into Comsol. We made a mistake by missing 2 shielding rods on the right, making the whole configuration not completely symmetric, but since they are far enough from the centre that we tried to investigate, it shouldn't cause a problem.

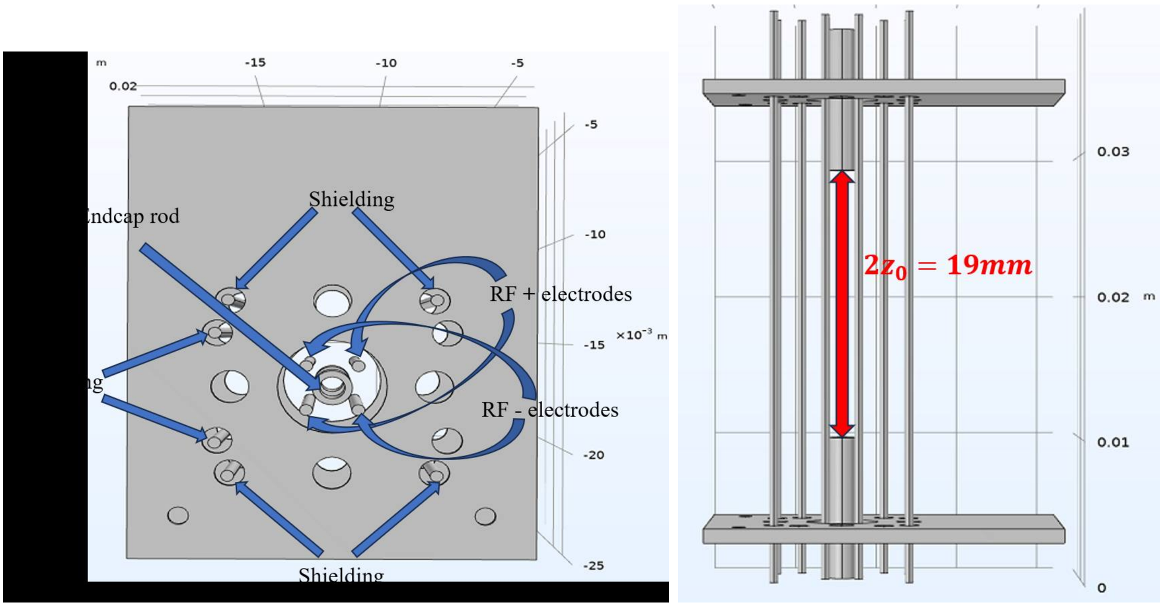

Figure A.3: Configuration of Paul trap in Comsol simulation (only metal parts are shown). Left: top view. RF +/- electrodes refer to the fact that each diagonal pair is connected to the same RF source, and two RF sources have a phase difference of π. Two shielding rods are missed (there are only 6 in the figure).
Right: side view. Distance between 2 endcaps is ca. 19 mm.

To calculate the approximated pseudopotential

$$V_{\text{eff}}(z) = \frac{1}{4m}(\frac{n_e e}{\Omega_{rf}})^2|E(z)|^2$$

, we ground all the shielding rods, plates and endcap tube rods, and apply DC voltages +/-V_{rf} (equal to RF amplitude that we want to apply in reality) respectively to RF +/- electrodes. And with the assistance of Comsol DC electric fields simulation we're able to attain the absolute value of the electric field in the radial centre along the axial z-direction, $E(z)$. Notice that this $E(z)$ includes x,y,z components, i.e. $\vec{E}(z) = (E_x(z), E_y(z), E_z(z))$. With absolute value of it, the rest steps are purely about calculation and actually irrelevant to Comsol as shown in 2.1.1.

Results in Fig. 2.3 were extracted under the condition that $V_{rf} = 300$ V, $\Omega_{rf} = 2\pi \times 25$ kHz, charge on nanoparticle $n_e = 100$, and 200 nm diameter nanoparticle is used. Estimation of these parameters as well as geometry deviate from the final experiments.

And we attribute the phenomenon of noisy (spiky) acceleration results to the fact that we didn't have enough datapoints of potential ahead, in other words, meshing of simulation model in Comsol wasn't fine enough. We found the solution in the last stage of our project that in Comsol meshing precision could actually be locally specified, therefore meshing of the centre axial line where we try to calculate value of the electric force can be intensified in order to get more datapoints. However, we didn't finish this since it didn't seem meaningful enough after we already got all the experimental results with our real Paul trap.

A.3 RF electronics

The original design of the electronics that provide high voltage RF signal to the RF electrodes of Paul trap is hard to reach a high voltage output at high frequency because of the misuse of

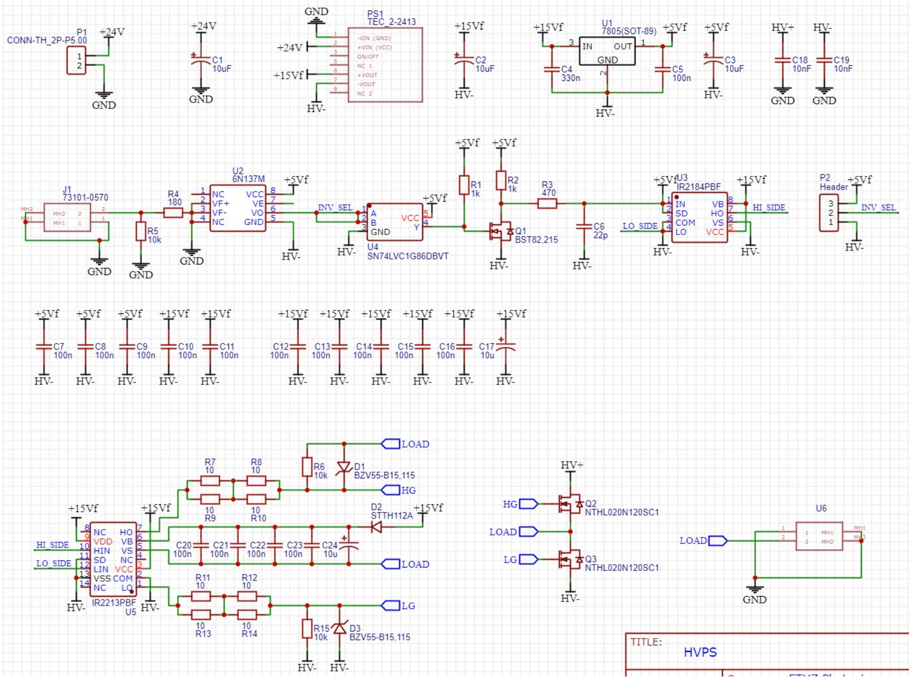

Figure A.4: The draft of circuit produced by Gabriele in his thesis[15]. Noted that the transistor NTHL020N120SC1 is not the correct one.

a high loss MOSFET. The requirement of loss can be understood by simply calculating the dissipating power of the MOSFET. The formula is simply $E = f * E_s$,where E,f,E_s is the total energy, the frequency and the switching loss respectively. From the formula, we learn that a higher energy loss requires more power from the power supply, which leads to a supply voltage drop. To make the circuit working upon 50kHz with 10W power supply, a limit of switch energy of 250 μJ is set. The original MOSFET NTHL020N120SC1 induces such voltage drop with F10CT since its switching loss is 3000 μJ, way too large that the desired one. AIMW120R060M1H show meets the design requirement with loss of around 260 μJ.

Figure.A.4 shows a complete design of the PCB circuit. P1 is a connector for 24 V power supply to the board. This voltage will be converted by PS1 (TEX_22413) to +15 VF compared to the virtual ground (in this case it is HV- = -500 V). VF stands for the voltage compared to the virtual ground value. 0 VF is -500 V in this PCB. Together with a +5 VF voltage generated by U1(7805 SOT-89), the components on the chip are powered up.

The signal input from J1 will first pass through a pull up resistor and a 180 ohm protection load. Inside 6N137M, a LED is lit according to the input signal. The emitted light is captured by another diode and transferred to a signal referring to the virtual ground. This optical coupler delivers the common ground input signal to virtual ground one. Although there exists controllable inner AND gate by pin7 of 6N137M, the original design presents a XOR gate outside as U4(SN74LVC1G86DBVT). By changing the connection of two pins in P2(Header), the phase of the signal can be 0 or 180 degree compared with the input signal. It passes through a buffer MOSFET circuit to ensure that the swing is 5 VF. Then a RC low pass filter takes the high frequency noise out.

The 5V signal that goes in U3(IR2184PBF) will be amplified to 15 V signal. And then IR2213 uses it to switch on and off between -500 V and +500 V of the MOSFET. A smart design used in this circuit is the capacitors in the output part of IR2213. Those serves as a bootstrap circuit that opens the HV+ gate. When the HV- gate is on, they are charged by a voltage difference of 15 V. When the HV+ gate is on, the voltage difference between them is exact V_{gs} of the HV+ MOSFET. As a result, the *ground* side of capacitor will be connected to HV+(+500 V). A level shifter inside IR2213 maintains the voltage on capacitor but keeps increasing the common ground voltage. In this process, the gate voltage difference is kept the same when the gate opens. Thus the high gate is open.

Because the output of the MOSFET drive is a current source, the switching time and energy loss is related to the driving load. Specific load value needs to be used to have good switching profile. A diode to reduce the transient overshot of a switch and a pull-up resistor to configure a final state were put on the output line.

In our setup, we found that the output signal oscillates strongly when the switch is on, as is shown in Fig.A.5. This implies some accidentally formed RLC circuit that has a transfer function with poles which is not very well controlled. It could be caused by a mismatch of the output impedance of the PCB, which may cause a backward reflection to circuit. We didn't put any filter to kill the electric noise. Those could be attributed to the reasons of the oscillation.

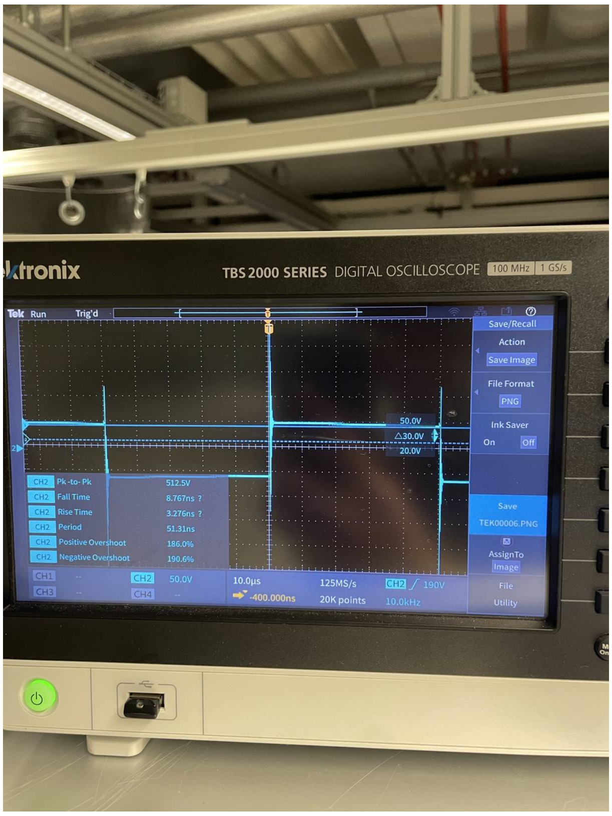

Figure A.5: The signal generated by one of the PCB measured on one of the trap electrodes. A significant overshoot and undershoot present. This shouldn't be a problem affects trapping since the time scale of this overshoot is less that 1 μs. Surely there is a better way to eliminate the overshoot, by inserting a capacitor to filter them out or shorten the connecting wire to reduce the inductance.

The output voltage verses the input voltage and power is shown on the left part of the Fig.A.6. A roughly linear relationship is found. On the picture on the right, the bandwidth can be found to be around 110kHz. Noted in the actual environment with load, the characteristic may change a Little. This changing shouldn't be detrimental to the PCB because the load is typically very small.

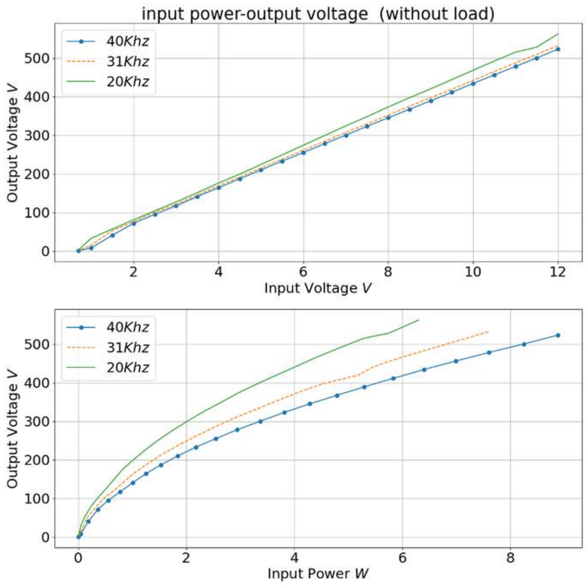

[redacted]

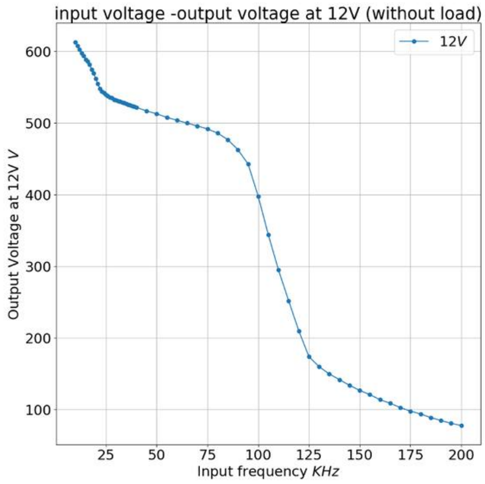

[redacted]

Figure A.6: PCB characteristic without load. Left, the output voltage with respective to the input voltage. Right, The output voltage verses input frequency. We can see that the circuit amplifier the input quite linearly for most of the input voltage. The bandwidth of the circuit is around 100kHz, which is a best case because no load is put when testing.

A.4 Endcap and DC electronics

In our new Paul trap, given the increased length, endcap potentials of tens of volts, if not hundreds, were expected to be needed to trap the particle in the axial direction. Furthermore, a requirement of the endcap voltages is the full control at any voltage (in order to implement a reloading control system and cooling of the particle) and fast switching off, because otherwise the particle would be affected during the fall by the decreasing potential and the measurement would be disturbed.

To meet all these requirements we decided to use an AWG combined with a fast high-voltage op-amp. The AWG that we ordered (Rigol DG-812), as well as most AWGs, could only output a few volts at maximum: we therefore planned on amplifying it with the op-amp. The choice for the op-amp fell on the HV264 Quad High-Voltage Amplifier Array by Microchip. It features 4 amplification channels (enough for the two endcaps and even potentially the two sets of compensation electrods) maximum voltage up to 200 V and slew rate of 9 V/µs, which corresponds to around 20 µs for the full ramp down from 200 V to 0 V, an acceptable compromise. Since the op-amp was delivered surface-mount, we designed and fabricated a PCB at the student project house of ETH to make it easily connectable with outside cables and soldered a low-current diode between two pins as suggested in the op-amp datasheet. Figure A.7 shows a picture of this. As a high-voltage source we used a step-up converter (A02P-24 by XP-power) that would convert 24 V in input into 200 V in output.

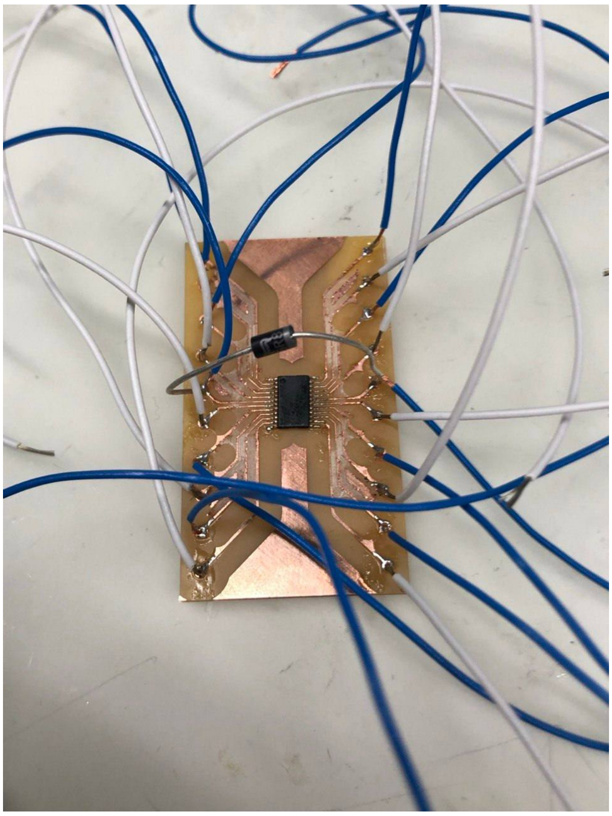

Figure A.7: Endcap voltage source: PCB with soldered the op-amp and the diode, and all the wires for the four channels and the voltage sources.

Initially when tested using a voltage generator in the workshop as high voltage source the circuit worked as expected. However, unfortunately, when we connected the step-up converter, this (for reason that was never understood) did not work, and as a result probably both the op-amp and the step-up converter got burned (I would suggest to verify this before throwing them away though). As an indication that the problem might lay in the op-amp, when we tried to connect another high voltage supply to the op-amp, even this voltage supply got burned. The high voltage supply (with a long turn-off time) was the one initially used to control the endcap voltages. Other two op-amps are available, as we had ordered three of them. The step-up converter, if broken, would have to be re-ordered, as we had only one of it.

We therefore never ended up using the AWG-and-op-amp combination to drive the endcaps, and this led us to not have a fast switch off of the voltage and thus one important cause of the corrupted value of measured gravitational acceleration in the experiments. With, the last day, the burning of the slow high-voltage supply, the setup currently misses a voltage supply for the endcaps.